Influence of cusp O^+ outflow on magnetotail dynamics in a multifluid MHD model of the magnetosphere

M. Wiltberger,[1] W. Lotko,[2] J. G. Lyon,[3] P. Damiano,[2] and V. Merkin[4]

Received 19 April 2010; revised 25 June 2010; accepted 30 June 2010; published 2 October 2010.

[1] A multifluid version of the Lyon-Fedder-Mobarry global simulation model has been used to investigate the effects of outflowing ionospheric O^+ on the magnetosphere-ionosphere system. To quantify these effects, we specify the number density, upward parallel velocity, and temperature of the O^+ outflow in a limited area of the low-altitude simulation boundary representing the projection of cusp, cleft, and low-latitude boundary layer. A baseline simulation without O^+ outflow is compared with simulations with a range of fluxes and initial velocities. In the cases with high fluxes, it is shown that the configuration of the magnetosphere is dramatically changed. In particular, the cross-polar cap potential is reduced, the polar cap area is increased, and the nightside reconnection line is moved earthward. Furthermore, in one case, the O^+ outflow leads to the onset of a second substorm not seen in the other simulation runs.

Citation: Wiltberger, M., W. Lotko, J. G. Lyon, P. Damiano, and V. Merkin (2010), Influence of cusp O^+ outflow on magnetotail dynamics in a multifluid MHD model of the magnetosphere, *J. Geophys. Res.*, *115*, A00J05, doi:10.1029/2010JA015579.

1. Introduction

[2] The high-latitude ionosphere is a persistent source of outflowing plasma and the only source of O^+ in the magnetosphere [*Yau and Andre*, 1997; *Chappell et al.*, 2000; *Bouhram et al.*, 2004]. Observations during active times have shown that O^+ can become the dominant component of the plasma sheet [*Peterson et al.*, 1981; *Kistler et al.*, 2005]. Several studies have indicated that O^+ could influence the substorm process by changing the growth phase [*Daglis et al.*, 1990] and affecting the initiation mechanism [*Baker et al.*, 1982; *Cladis and Francis*, 1992; *Lakhina*, 1995]. However, the global consequences of this plasma on the magnetosphere-ionosphere system are difficult to evaluate observationally [*Lotko*, 2007].

[3] Microscale simulations of magnetic reconnection by *Shay and Swisdak* [2004] indicate that the reconnection rate in a multifluid plasma is lower than in a single-fluid plasma, with the implication for magnetotail dynamics that substorms will either need to occur more frequently or exhibit longer expansion phases to maintain global flux balance. *Winglee et al.* [2002] used a multifluid model of the magnetosphere and a gravitationally bound source of O^+ to study the impact of outflows on the magnetosphere during a storm. They found that O^+ outflows reduce the cross-polar cap potential and the polar cap area. *Glocer et al.* [2009] developed a Polar Wind Outflow Module (PWOM) for the Space Weather Modeling Framework and showed that its inclusion results in stronger *Dst* and reduced polar cap potentials in the model results. In this work we use the recently developed MultiFluid Lyon Fedder Mobarry (MFLFM) model (J. G. Lyon and V. Merkin, Multifluid equations for MHD, submitted to *Journal of Geophysical Research*, 2010) to simulate the effects of a fixed cusp-region outflow on the evolution of the magnetosphere.

[4] This paper begins with a brief introduction to the MFLFM model in section 2. This section also contains a detailed discussion of how the cusp O^+ outflow is included into the model. Section 3 presents the results from model for a series of runs with different values for the flux and velocity of the plasma in the cusp outflow. In section 4 we discuss these results before summarizing our conclusions in section 5.

2. Modeling Methodology

2.1. Multifluid MHD Model

[5] The MFLFM builds upon the techniques used in the standard one-fluid LFM [*Lyon et al.*, 2004] to produce a multifluid approach that allows each species to move under its own force balance. The MFLFM code solves

$$\frac{\partial \rho_\alpha}{\partial t} = -\nabla \cdot \rho_\alpha \vec{u}_\alpha, \tag{1}$$

$$\frac{\partial \vec{p}_\alpha}{\partial t} = -\nabla \cdot \left(\vec{P}_\alpha \vec{u}_\alpha + \underline{I} P_\alpha\right) + \vec{F}^d_\alpha + n_\alpha q_\alpha \vec{E}_\parallel, \tag{2}$$

$$\frac{\partial \mathrm{E}_\alpha}{\partial t} = -\nabla \cdot \vec{u}_\alpha (\mathrm{E}_\alpha + \mathrm{P}_\alpha) + \vec{u}_\alpha \cdot \left(\vec{F}^d_\alpha + n_\alpha q_\alpha \vec{E}_\parallel\right), \tag{3}$$

[1]High Altitude Observatory, National Center for Atmospheric Research, Boulder, Colorado, USA.
[2]Thayer School of Engineering, Dartmouth College, Hanover, New Hampshire, USA.
[3]Department of Physics and Astronomy, Dartmouth College, Hanover, New Hampshire, USA.
[4]Center for Integrated Space Weather Modeling, Boston University, Boston, Massachusetts, USA.

0148-0227/10/2010JA015579

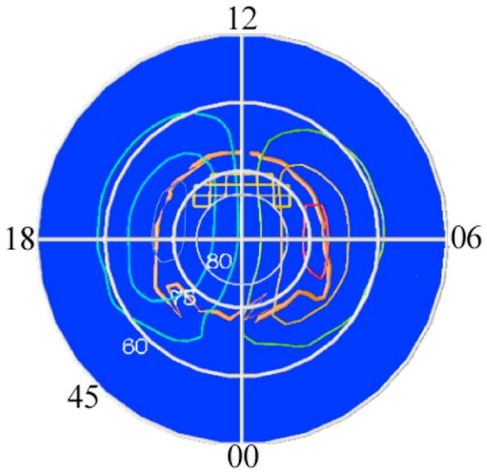

Figure 1. The grid cells of the specified outflow region are highlighted in yellow in this view of the northern ionosphere at simulation time 0300 ST. The orange line is the boundary between open and closed magnetic field lines. The colored contours on the blue background represent the cross-polar cap potential pattern.

$$\frac{\partial \vec{B}}{\partial t} = -\nabla \times (\vec{u} + \vec{B}), \tag{4}$$

with ambipolar field $\vec{E}_{\|} = \hat{b}\hat{b} \cdot \nabla P_e / ne$, and Lorentz force due to the first-order ion drift given by

$$\vec{F}^d_\alpha \equiv \hat{b} \times \left[\vec{p_\alpha} \cdot \nabla \vec{u}_\alpha + \nabla P_\alpha + \frac{\rho_\alpha (\vec{u}_M - \vec{u}_\alpha) \cdot \hat{b}}{B} \frac{\partial \vec{B}}{\partial t} - \frac{\rho_\alpha}{\rho} \left(\sum_\beta (\vec{p}_\beta \cdot \nabla \vec{u}_\beta + \nabla P_\beta) + \nabla P_e - \vec{j} \times \vec{B} \right) \right] \times \hat{b}. \tag{5}$$

Subscripts α and β designate ion species. P_e is the pressure of the inertialess electrons; n_α, ρ_α, $\vec{u}_\alpha$, and P_α are the ion number density, mass density, velocity and partial pressure; $n = \sum_\alpha n_\alpha$ is the plasma number density; $\rho = \sum_\alpha m_\alpha n_\alpha$ is the mass density; $\vec{u}$ is the ion center of mass velocity. $\underline{I}$ is the identity tensor, and $\hat{b} = \vec{B}/B$. Parameters include ion charge q_α, ion mass m_α, and electron charge e.

[6] Equations (1)–(3) evolve the densities of ion mass ($\rho_\alpha = m_\alpha n_\alpha$), momentum ($\vec{p}_\alpha \equiv \rho_\alpha \vec{u}_\alpha$), and plasma energy ($E_\alpha = \frac{1}{2}\rho_\alpha u_\alpha^2 + P_\alpha/(\gamma - 1)$). Equation (4) is Faraday's law for ideal MHD. The standard MHD ordering [*Kulsrud*, 1983] used to derive these equations constrains all ion species to move in the perpendicular direction with the $\vec{E} \times \vec{B}$ velocity. The time rate of change of $\vec{B}$ in $\vec{F}^d_\alpha$ effects momentum transfer between species when the field direction changes. Because $\sum_\alpha \vec{F}^d_\alpha = -\nabla_\perp P_e + \vec{j} \times \vec{B}$, summing (1)–(3) over species yields one-fluid MHD less electron inertia.

[7] The ambipolar electric field, $\vec{E}_{\|}$, depends upon the electron plasma pressure. Observationally the electron pressure is a fraction of the ion pressure. In order to simplify the analysis of these runs we have chosen to set the electron pressure equal to zero, which means that there is no ambipolar electric field in these runs. This has the net effect of removing counterstreaming interactions between the plasma species. The interested reader is encouraged to read Lyon and Merkin (submitted manuscript, 2010) for a more detailed discussion of this term as well as a detailed derivation of all the equations used in the MFLFM. *Brambles et al.* [2010] show that the counterstreaming interaction only occurs over a short interval above the boundary in the cusp before the flow enters the lobe where the low H^+ density implies the electron pressure will be small, and therefore neglecting this term is not likely to have significant impact on the results presented in this paper.

2.2. Ionospheric Outflow Model

[8] The main goal here is to investigate the consequences of O^+ outflow on the magnetospheric configuration and on the magnetosphere-ionosphere interaction using MFLFM model while side-stepping the difficult problem of how ionospheric O^+ is accelerated to escape velocity in forming an outflow. To specify a plausible outflow, we turn to observations to answer two fundamental questions: (1) Where does ionospheric outflow occur, and (2) what are the typical properties of this outflow? In addressing these questions, we focus only on the largest and most persistent source persistent source of O^+ outflow, which is the dayside cusp/cleft region.

[9] *Lennartsson et al.* [2004] used POLAR to study O^+ outflow rates during an interval near solar minimum to show that statistically the most intense O^+ outflows occur in a cusp-like region on the dayside, extending from approximately 80° to 75° invariant latitude and from 9 to 13 h magnetic local time (MLT). *Andersson et al.* [2005] conducted a similar analysis using the FAST spacecraft and found that area of the outflow increases in MLT with increasing height. These dayside outflows are statistically coincident with the region of soft electron precipitation originating in the low-latitude boundary layer (LLBL), cusp, and mantle regions identified by *Newell and Meng* [1992] from DMSP data. In Figure 1 we show the ionospheric mapping of the low-altitude, boundary simulation cells through which the specified outflow enters the simulation domain. Potential contours and the projection of the open-closed field line boundary at 0300 simulation time (ST) in the simulations discussed below are also indicated. This area corresponds approximately to the statistical patterns derived from the observations and lies a few degrees poleward of the dayside portion of the open-closed field line boundary.

[10] The inner boundary of the MFLFM computational domain is a sphere of geocentric radius 2 R_E. On this boundary we fix the density, velocity, and temperature of the O^+ fluid in order to specify the flux coming from the outflow cells shown in Figure 1. Outside the outflow region a hard wall boundary condition is imposed. The choice of outflow parameters is motivated by the following observations. In analyzing cusp region O^+ data from the Akebono, Interball 2, and Cluster satellites up to altitudes of 5.5 R_E, *Bouhram et al.* [2004] report that the upward parallel velocity of the outflow exhibits considerable scatter at all altitudes considered, with velocities ranging from 20 to 100 km near 2.8 R_E geocentric, the lowest altitude for which they reported bulk parallel velocities. The temperatures of the outflow range from 10 to 100 eV with a linear trend from 1.5 to 4 R_E geocentric, with 10 eV being typical near 1.5 R_E geocentric. *Bouhram et al.* [2004] do not provide an altitude profile for

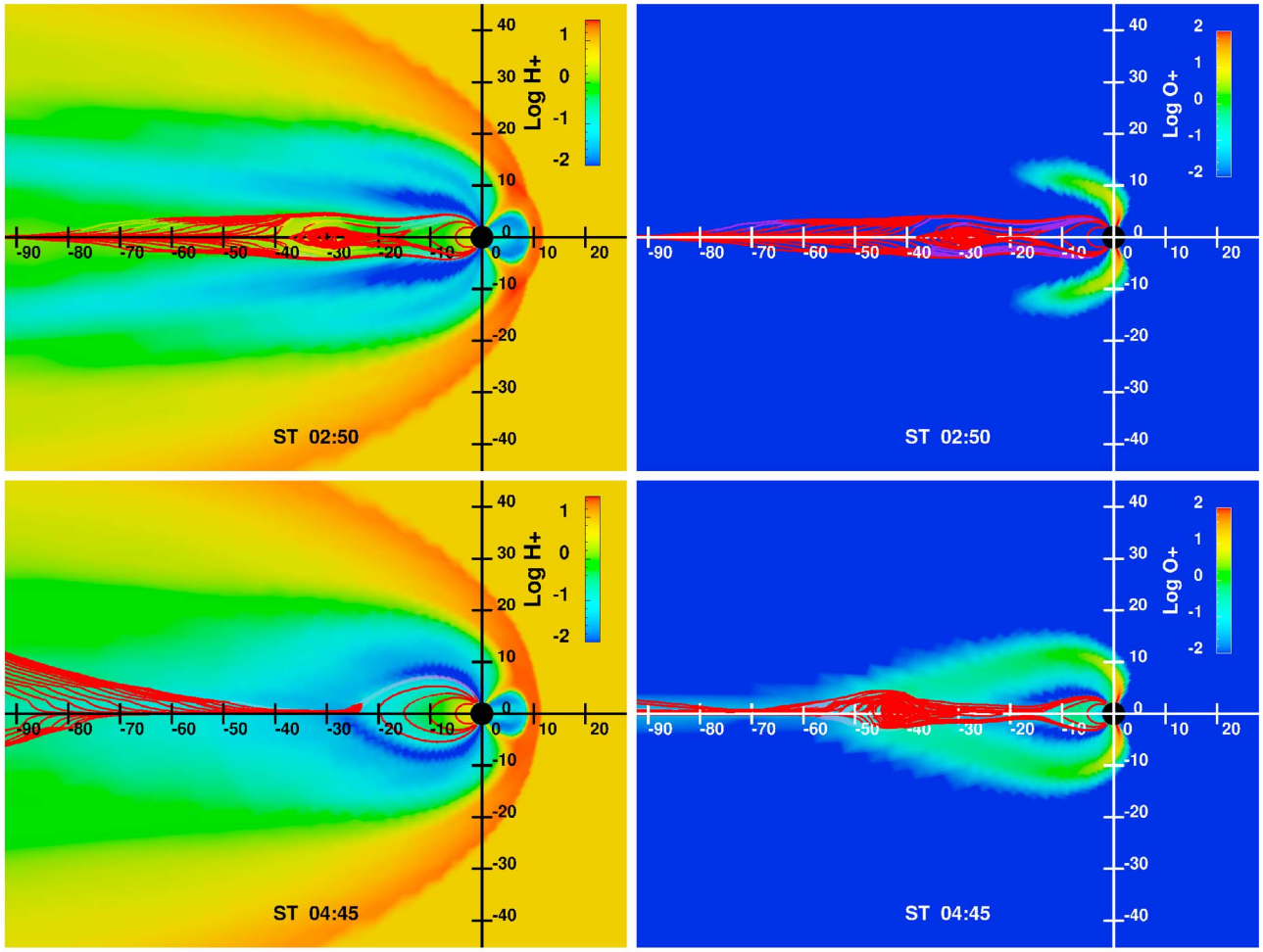

Figure 2. A comparison of the magnetospheric configuration for a run (left) without and (right) with O^+ outflow. (top) The configuration during the first substorm interval. (bottom) A second substorm is only seen in the SFE9 outflow simulation.

the density, but during one event observed by Cluster near 4 R_E, the density was given as 0.1 cm^{-3} with an upward velocity of 100 km/s, corresponding to a flux of $10^6/cm^2$ s. The climatological O^+ fluxes reported by *Lennartsson et al.* [2004] for Polar perigee passes near 2 R_E geocentric peak at about $10^8/cm^2$ s when projected to 300 km altitude assuming flux conservation. This peak flux would map to a value of $10^7/cm^2$ s at the Polar perigee altitude. Using FAST satellite data taken near 4000 km altitude, *Strangeway et al.* [2005] report cusp-region fluxes ranging from 10^6 to $10^9/cm^2$ s during the 24–25 September 1998 storm interval. *Bouhram et al.* [2004] note that the density and flux of the outflow vary significantly with solar cycle, while the parallel velocity and temperature exhibit less variance with solar cycle.

[11] Given the range of fluxes and velocities reported by these studies, we have chosen to conduct simulations with three different specifications of the outflow parameters. In the first simulation, we target a flux of $10^9/cm^2$ s by setting the outflow velocity to be 20 km/s with a density of 500 cm^{-3}. In the second simulation we maintain the same flux but increase the outflow velocity to 50 km/s, which requires us to reduce the density in the outflow region to 200 cm^{-3}. In the third simulation we reduce the flux to $10^7/cm^2$ s by keeping the velocity at 20 km/s but reducing the density to 5 cm^{-3}. In all cases we keep the O^+ temperature in the outflow cells fixed at 10 eV. Because the first simulation has a slow outflow velocity and flux of 10^9, we will refer to it as the SFE9 run. The second simulation has a fast outflow velocity, so we will refer to it as the FFE9 run, and following this same convention the third simulation run will be called the SFE7 run.

[12] The MFLFM model with two ion fluids is used to study the effects of outflow. The first fluid is the solar wind plasma composed of protons. The density, velocity, and sound speed of this plasma are held fixed during simulation intervals at 5 cm^{-3}, 400 km/s, and 40 km/s, respectively. At the beginning of the simulation (0000 ST) the IMF is southward at 5 nT and remains so for 1 h before turning northward. At 0200 ST the IMF points southward again and remains southward for the remainder of the simulation. Also at 0200 ST the O^+ fluid first begins flowing into the simulation domain from the outflow boundary region for each of

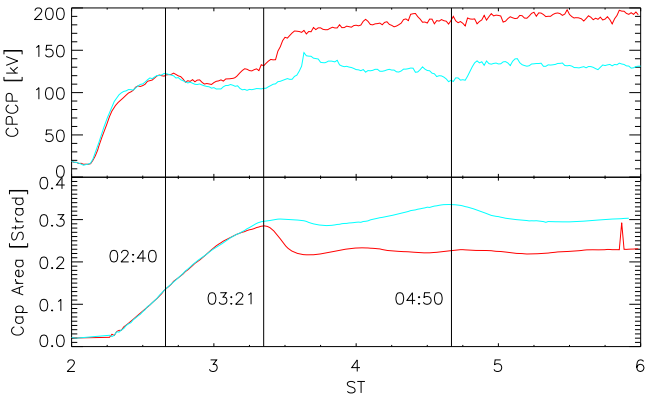

Figure 3. Comparison of the baseline (red) and SFE9 outflow (cyan) simulation results. The cross-polar cap potential (CPCP) is shown at top, while the polar cap area is shown at the bottom.

the three outflow simulations. For reference, the MFLFM was also run with a single fluid and no outflow under the same solar wind conditions, which we will refer to as the baseline run.

3. Results

[13] Figure 2 shows the comparison between the MFLFM baseline and SFE9 runs produced with the CISM-DX package [*Wiltberger et al.*, 2005]. The baseline run without outflow is shown in Figure 2 (left) with a cut through the XZ plane colored by the $\log_{10}$ of the proton (H^+) density. The basic structure of the magnetosphere is quite apparent here with a clearly defined magnetopause and bow shock on the dayside and a plasma sheet on the nightside. In Figure 2 (right), the XZ plane is colored with the $\log_{10}$ of the O^+ density for the SFE9 run with ionospheric outflow. Because the only source of O^+ is the cusp-cleft outflow region, the majority of the plane is blue, indicating no O^+ plasma, while the expansion and tailward stream of the outflow is clear. In both cases, magnetic field lines are traced from points every 5 R_E along the X axis from −80 to −5 R_E.

[14] After the IMF turns southward the magnetotail begins to thin, and eventually a near-Earth reconnection line forms near $X = -25$ R_E. At 0250 ST (Figure 2, top), a plasmoid is evident in the magnetic field configuration of both simulations. In the case with ionospheric outflow the visualization clearly shows that the O^+ has not yet reached the central plasma sheet. In fact, it does not do so until approximately 0320 ST. In both cases the plasmoid forms, propagates tailward, and exits into the solar wind from the tailward boundary. This evolution is typical for LFM simulations with steady southward IMF. It is also worth noting that while not shown, the H^+ configuration in the outflow simulation is virtually identical to the simulation without outflow.

[15] The configurations of the two systems at 0445 ST are shown in Figure 2 (bottom). In the baseline run, the typical quasi-steady configuration has developed with a reconnection line persisting near $X = -30$ R_E. In contrast, the configuration for the outflow run in Figure 2 (right) is very different. A new near-Earth reconnection region has formed earthward of $X = -20$ R_E, and a new plasmoid is evident. This plasmoid is eventually released from the magnetosphere in a fashion similar to the initial substorm sequence seen in both simulations. This cycle does not appear to repeat indefinitely. After this plasmoid is released, the simulated magnetosphere reaches a new dynamic steady state with the last closed field line occurring near $X = -20$ R_E. The outflow from the ionosphere subsequently lands tailward of this reconnection line, and the bulk of the O^+ ions continue to flow down the magnetotail. This shorter magnetotail also affects the distribution of H^+ in the outflow simulation; as expected, it remains confined to the closed field region and has slightly higher densities than the baseline simulation.

[16] Figure 3 compares the cross-polar cap potential (CPCP) in the ionosphere and the polar cap area for the baseline and SFE9 outflow simulations. These results exhibit two very clear trends. During the initial period after the southward turning of the IMF, the CPCP in the two simulations increases at the same rate to a peak value of approximately 120 kV at 0240 ST before stabilizing in both simulations. Later in the runs, both simulations asymptote

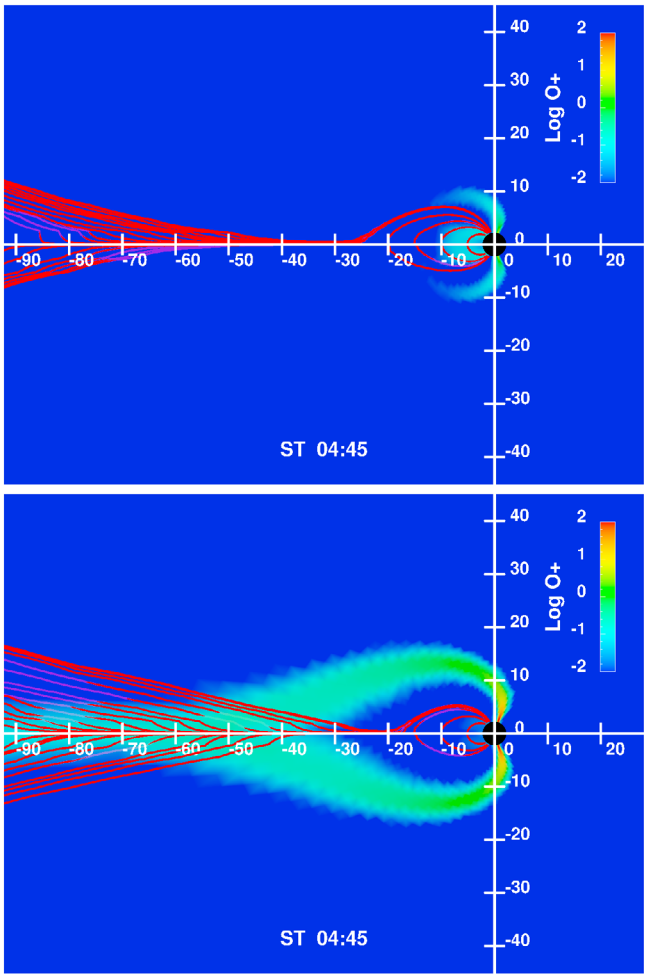

Figure 4. Configuration of the magnetotail in the (top) SFE7 and (bottom) FFE9 simulations at 0445 ST. These frames are in the same format as the right-hand plots of Figure 2.

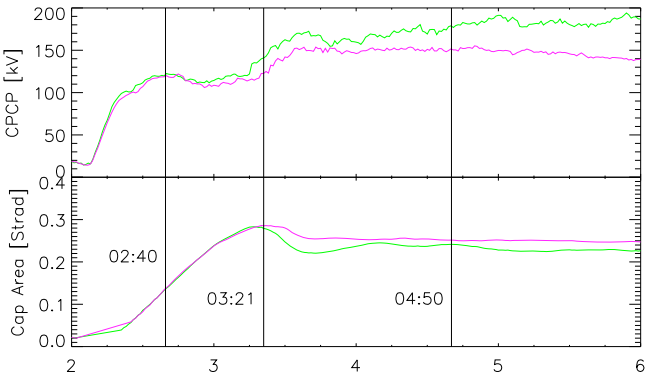

Figure 5. Comparison of the SFE7 (green) and FFE9 outflow (purple) simulation results. The cross-polar cap potential (CPCP) is shown at top, while the polar cap area is shown at the bottom.

to a quasi-steady CPCP but on different time scales and to different asymptotic values. In the baseline simulation, the asymptotic potential is approximately 190 kV, while in the SFE9 outflow simulation the potential is reduced to 130 kV. The polar cap area shows a clear increase after the imposition of southward IMF. In the baseline simulation it reaches a peak value at 0321 ST. At this time the plasmoid that formed much earlier has now passed through $X = -60\ R_E$. This peak marks the end of the initial increase in the CPCP. In the SFE9 simulation with outflow, the peak in open area occurs approximately 6 min after the peak in the baseline simulation. The different time histories of the polar cap area after the release of the first plasmoid reflect the differences seen in the magnetotail structure. The polar cap area modestly increases in the SFE9 outflow simulation from about 0345 ST until 0450 ST when the second plasmoid is finally released. The decrease in area after this plasmoid exits is not as abrupt or large as seen in the first sequence. The polar cap area asymptotes at a higher level in the SFE9 outflow run than in the baseline run, which is a reflection of the fact that the nightside reconnection line is closer to the Earth in the SFE9 outflow simulation. Note that the small blip seen the baseline run around 0540 ST is the results of a minor miscalculation in polar cap area algorithm.

[17] The evolution of the magnetotail is similar to the baseline case for the FFE9 and SFE7 simulations. In Figure 4 we show the configuration of the magnetotail at 0445 ST. In the SFE9 simulation the plasmoid from the second substorm was clearly evident, but it is not present in either of these runs. In the FFE9 simulation we can clearly see that flow from the cusp is landing tailward of the reconnection site formed during the first substorm. It is also important to note that the reconnection site has move earthward, approximately 8 R_E, from the position shown at this time for the baseline simulation shown in Figure 2. It is also clear that very little of the O^+ plasma from the plume is making it into the inner magnetosphere. The SFE7 also does not have a second plasmoid, but in this case it is due to the fact that the slower outflow does not reach the magnetotail reconnection site. Some O^+ does make it into the inner magnetosphere when the open field lines it is traveling on become closed during the ejection of the plasmoid formed during the initial substorm event. This plasma remains trapped, but it is not contributing significantly to total plasma pressure, as is evident by the very similar configuration of the magnetotail field lines, including the location of the reconnection site, in this simulation and the baseline run. The H^+ distributions in both of these simulations are very similar to the baseline simulation with the FFE9 having the same density profile constrained to a slightly smaller closed field region.

[18] The similar evolution between the FFE9 and SFE7 simulations and the baseline simulation can also been seen in the comparison of the CPCP and polar cap area displayed in Figure 5. In both of these cases the CPCP reaches a peak value of 120 kV at 0240 ST before stabilizing just as the baseline and SFE9 simulations. After approximately 0315 ST the behavior of the CPCP tracks differ between these two runs. In the SFE7 run the CPCP tracks the baseline run, reaching a slightly lower, 185 kV, asymptotic value for the potential. The CPCP potential is slightly higher than the baseline event between 0315 and 0330 ST but is lower than the baseline run for the remainder of the interval. In the FFE9 event the initial track of the CPCP is quite similar to the SFE7 and baseline simulations, but after 0315 the CPCP remains significantly lower than the baseline case and asymptotes at a value of 145 kV which is approximately 10–15 kV higher than the asymptotic value for the SFE9 simulation. The polar cap area data displayed in Figure 5 also support the conclusion that no second substorm occurred in either of these simulations. In both of these events the polar cap area increases until 0321 ST and then decreases until it reach a quasi-stable value. The SFE7 area is nearly identical to the area seen in the baseline simulation, with it being slightly higher for the hour after 0400 ST and the peak occurring a few minutes earlier. In the FFE9 case the peak is delayed by a few minutes and has a higher quasi-stable value for the polar area. In neither case is the increase in polar area seen during the second substorm sequence in the SFE9 simulation evident.

4. Discussion

[19] The profound differences that result when plasma of ionospheric origin is included in the SFE9 simulation may be interpreted as follows. The O^+ plume lands near the initial reconnection region of the first substorm, with the bulk of the O^+ plasma intersecting the magnetotail current sheet significantly earthward of the location of the quasi-steady reconnection region in the simulation without outflow. The additional plasma carried into the plasma sheet by the outflow affects the dynamics in two ways. First, it changes the reconnection rate, evidenced by the 6 min delay in the final release of the first plasmoid. The reconnection rate is proportional to the Alfvén speed in the fluid flowing into the reconnection diffusion region, so a reduction in the reconnection rate is expected in the simulation with outflow owing to the reduction in Alfvén speed caused by the O^+ ions in the lobe inflow region. Second, the O^+ ions add an additional source of plasma that assists in repopulating the plasma sheet. The combination of these effects prevents the simulated magnetosphere with outflow from settling into the typical quasi-steady equilibrium. While it will be necessary to perform a simulation with an H^+ outflow with the same mass flux to determine the relative importance of these

two factors, we suspect that the refilling of the plasma sheet is the more significant effect. The other significant difference is the dramatic reduction in the CPCP in the run with O^+ outflow. This reduction appears to be due to a global reduction in the intensity of the region 1 field-aligned currents and is likely linked to changes in the conductance resulting from the increased plasma density at the low-altitude simulation boundary and its effects on the electron precipitation derived from the LFM precipitation model [*Fedder et al.*, 1995]. As suggested by *Winglee et al.* [2002], another contributing factor may be the mass loading of the magnetosphere by the O^+ outflow. To isolate this effect, we will have to perform another series of simulations without electron precipitation, i.e., with fixed ionospheric conductance.

[20] It is also clear from these simulations that the impact of O^+ outflow depends heavily on the parameters of the plasma entering the magnetosphere. In the FFE9 simulation the initial velocity of the O^+ is increased to 50 km/s, which is sufficient to allow the plasma to advect farther down the magnetotail during the time the field lines are being convected across the polar cap. This additional distance traveled results in the plasma landing tailward of near-Earth reconnection site setup during the first substorm in the simulation. As already noted, this configuration prevents significant O^+ plasma from entering the inner magnetosphere, and since no second substorm is observed, this provides additional support for the argument that the refilling of the plasma sheet seen in the SFE9 simulation is the most significant effect leading to the onset of a second substorm. The SFE7 simulation also shows no substorm, but in this case it is just due to the reduced flux not being large enough to contribute significant amounts of plasma to the magnetosphere. It is also important to note here that the fixed solar wind parameters driving the magnetosphere results in a quasi-stable location of the midtail reconnection site, and more realistic solar wind conditions are likely to be much more variable, increasing the likelihood that the O^+ plasma plume will have a chance to interact with the reconnection site. Another intriguing possibility is the interplay between plasma from the nightside, which could help refill the plasma sheet and potentially force the reconnection site tailward into the plume from the cusp.

[21] As a final point of discussion, we note that in the simulations reported by *Winglee et al.* [2002], the ionosphere is represented as a thin resistive layer at the low-altitude simulation boundary. The resistivity is constant in the layer so outflow-induced changes in the fluid density near the boundary have no effect on the conductance of the layer, i.e., the effective ionospheric conductance. In the actual magnetosphere-ionosphere interaction, parallel potential drops develop in low-density regions near 1 R_E altitude in order to sustain the field-aligned current flowing through the low-density region [*Fridman and Lemaire*, 1980]. These potentials accelerate precipitating electrons, which increases their energy flux and ionizing effect on the ionosphere and on the ionospheric conductivity. If outflows are stimulated on field lines where parallel potentials also occur, the resulting upward flux of ions increases the plasma density in such regions and, to some extent, ameliorates the need for parallel potentials. The LFM precipitation model captures this nonlinear feedback that is absent when the ionosphere is represented as a constant resistive layer. Determining the relative contribution of this nonlinear feedback process in regulating the CPCP compared to the mass loading of magnetospheric convection by a heavy ion outflow will require further investigation.

5. Conclusions and Future Work

[22] The effect of ionospheric O^+ outflow on magnetospheric dynamics has been investigated using the MFLFM model for the solar wind-magnetosphere-ionosphere interaction. While the outflow model is simplistic, it does place outflowing O^+ in the region of the cusp where it is statistically prevalent in satellite observations. The velocity and flux of the outflowing plasma were selected to sample conditions present in the vast range of observations. The introduction of intense outflow fluxes can have a profound effect on the evolution of the simulated magnetosphere, namely, a second substorm sequence is seen in one outflow simulation while quasi-steady equilibrium is reached after the first substorm sequence in the simulation without outflow. In addition to this major change, we observe a short delay in the release of the plasmoid for the first substorm sequence and a significant reduction in the cross-polar cap potential when high flux levels of ionospheric O^+ outflow are included in the simulation. Smaller fluxes are shown not to have significant impact on the structure and evolution of magnetotail.

[23] These simulations represent an important step in including ionospheric outflow in global simulations of the electrodynamically coupled magnetosphere-ionosphere system. More realistic simulations will require causal regulation of the outflow by a self-consistently evolving, coupled magnetosphere and ionosphere. *Brambles et al.* [2010], also in this special issue, uses the MFLFM during a modest magnetic storm interval to begin these investigations. We also need to conduct a detailed analysis of the impact of O^+ on the reconnection rate in the magnetosphere.

[24] **Acknowledgments.** This material is based upon work supported by CISM, which is funded by the STC program of the National Science Foundation under agreement ATM-0120950 and by NASA grants NAG5-12652, NNG056J706, NNX07AQ16G, NNX08AI36G, and NNX09AM49G. The National Center for Atmospheric Research is sponsored by the National Science Foundation.

[25] Masaki Fujimoto thanks Andrew Yau and another reviewer for their assistance in evaluating this paper.

References

Andersson, L., W. K. Peterson, and K. M. McBryd (2005), Esitimates of the superthermal O^+ outflow characteristic energy and relative location in the auroral oval, *Geophys. Res. Lett.*, *32*, L09104, doi:10.1029/2004GL021434.

Baker, D. N., E. W. Hones Jr., D. T. Young, and J. Birn (1982), The possible role of ionospheric oxygen in the initiation and development of plasma sheet instabilities, *Geophys. Res. Lett.*, *9*(12), 1337–1340, doi:10.1029/GL009i012p01337.

Bouhram, M., B. Klecker, W. Miyake, H. Reme, J. A. Sauvaud, M. Malingre, L. Kistler, and A. Blagau (2004), On the altitude dependence of transversely heated O^+ distributions in the clusp/cleft, *Ann. Geophys.*, *22*, 1787–1798.

Brambles, O. J., W. Lotko, P. A. Damiano, B. Zhang, M. Wiltberger, and J. Lyon (2010), Effects of causally driven O+ cusp outflow on the magnetosphere-ionosphere system using a multifluid global simulation, *J. Geophys. Res.*, doi:10.1029/2010JA015469, in press.

Chappell, C. R., B. L. Giles, T. E. Moore, D. C. Delcourt, P. D. Craven, and M. O. Chandler (2000), The adequacy of the ionospheric source in supplying magnetospheric plasma, *J. Atmos. Sol. Terr. Phys.*, *62*, 421–436.

Cladis, J. B., and W. E. Francis (1992), Distribution in magnetotail of O^+ ions from cusp/cleft ionosphere: A possible substorm trigger, *J. Geophys. Res.*, *97*(A1), 123–130, doi:10.1029/91JA02376.

Daglis, I. A., E. T. Sarris, and G. Kremser (1990), Indications for ionospheric participation in the substorm process from AMPTE/CCE observations, *Geophys. Res. Lett.*, *17*(1), 57–60, doi:10.1029/GL017i001p00057.

Fedder, J. A., S. P. Slinker, J. G. Lyon, and R. D. Elphinstone (1995), Global numerical simulation of the growth phase and the expansion onset for substorm observed by Viking, *J. Geophys. Res.*, *100*(A10), 19,083–19,093, doi:10.1029/95JA01524.

Fridman, M., and J. Lemaire (1980), Relationship between auroral electron fluxes and field aligned electric potential difference, *J. Geophys. Res.*, *85*(A2), 664–670, doi:10.1029/JA085iA02p00664.

Glocer, A., G. Töth, T. Gombosi, and D. Welling (2009), Modeling ionospheric outflows and their impact on the magnetosphere, initial results, *J. Geophys. Res.*, *114*, A05216, doi:10.1029/2009JA014053.

Kistler, L. M., et al. (2005), Contribution of nonadiabatic ions to the cross-tail current in an O^+ dominated thin current sheet, *J. Geophys. Res.*, *110*, A06213, doi:10.1029/2004JA010653.

Kulsrud, R. M. (1983), MHD description of plasma, in *Handbook of Plasma Physics*, *Basic Plasma Physics*, vol. 1, edited by M. N. Rosenbluth and R. Z. Sagdeev, pp. 115–145, North-Holland, New York.

Lakhina, G. S. (1995), Excitation of plasma sheet instabilities by ionospheric O^+ ions, *Geophys. Res. Lett.*, *22*, 3453–3456, doi:10.1029/95GL03427.

Lennartsson, O. W., H. L. Collin, and W. K. Peterson (2004), Solar wind control of Earth's H^+ and O^+ outflow rates in the 15-eV to 33-keV energy range, *J. Geophys. Res.*, *109*, A12212, doi:10.1029/2004JA010690.

Lotko, W. (2007), The magnetosphere ionosphere system from the perspective of plasma circulation: A tutorial, *J. Atmos. Sol. Terr. Phys.*, *69*, 191–211, doi:10.1016/j.jastp.2006.08.011.

Lyon, J. G., J. G. Fedder, and C. M. Mobarry (2004), The Lyon-Fedder-Mobarry (LFM) global MHD magnetospheric simulation code, *J. Atmos. Sol. Terr. Phys.*, *66*, 1333–1350, doi:10.1016/j.jastp.2004.03.020002E.

Newell, P. T., and C. I. Meng (1992), Mapping the dayside ionosphere to the magnetosphere according to particle precipitation characteristics, *Geophys. Res. Lett.*, *19*(6), 609–612, doi:10.1029/92GL00404.

Peterson, W. K., R. D. Sharp, E. G. Shelley, R. G. Johnson, and H. Balsiger (1981), Energetic ion composition of the plasma sheet, *J. Geophys. Res.*, *86*, 761–767.

Shay, M. A., and M. Swisdak (2004), Three-species collisionless reconnection: Effect of O^+ on magnetotail reconnection, *Phys. Rev. Lett.*, *93*(17) 175001, doi:10.1103/PhysRevLett.93.175001.

Strangeway, R. J., R. E. Ergun, Y. J. Su, C. W. Carlson, and R. C. Elphic (2005), Factors controlling ionospheric outflows as observed at intermediate altitudes, *J. Geophys. Res.*, *110*, A03221, doi:10.1029/2004JA010829.

Wiltberger, M., R. S. Weigel, M. Gehmeyr, and T. Guild (2005), Analysis and visualization of space science model output and data with CISM-DX, *J. Geophys. Res.*, *110*, A09224, doi:10.1029/2004JA010956.

Winglee, R. M., D. Chua, M. Brittnacher, G. K. Parks, and G. Lu (2002), Global impact of ionospheric outflows on the dynamics of the magnetosphere and cross-polar cap potential, *J. Geophys. Res.*, *107*(A9), 1237, doi:10.1029/2001JA000214.

Yau, A. W., and M. Andre (1997), Source of ion outflow in the high latitude ionosphere, *Space Sci. Rev.*, *80*, 1–25.

P. Damiano and W. Lotko, Thayer School of Engineering, Dartmouth College, 8000 Cummings Hall, Hanover, NH 03755, USA. (peter.damiano@dartmouth.edu; wlotko@dartmouth.edu)

J. G. Lyon, Department of Physics and Astronomy, Dartmouth College, 6127 Wilder Laboratory, Hanover, NH 03755, USA. (lyon@tinman.dartmouth.edu)

V. Merkin, Center for Integrated Space Weather Modeling, Boston University, 725 Commonwealth Ave., Boston, MA 02215, USA. (vgm@bu.edu)

M. Wiltberger, High Altitude Observatory, National Center for Atmospheric Research, 3080 Center Green, Boulder, CO 80301, USA. (wiltbemj@ucar.edu)